Virology Journal

RESEARCH

Open Access

An immune-based predictive model for HBV clearance: validation in multicenter cohorts and mechanistic insights from in vivo studies

Rongzheng Zhang[1†], Han Qiao[1†], Kun Zhou[1,2†], Xiaomei Ju[3], Xinyang Cao[1], Jianming Dong[4], Meng Wu[1], Le Yu[1] and Shuyun Zhang[1*]

Abstract

Background Chronic HBV infection is a major risk factor for hepatocellular carcinoma, posing a significant global health burden. However, predictive models for HBV clearance based on immune biomarkers remain limited.

Methods We systematically developed a predictive tool by quantifying mRNA expression levels of $CD4^+$ T-cell subset transcription factors, cytokines, and immune checkpoints in PBMCs from chronic HBV patients and resolved HBV individuals using RT-qPCR. A binary logistic regression model was constructed in the training cohort, with performance evaluated by ROC and calibration curves, followed by internal and external validation in independent cohorts. For in vivo validation, an HBV-transfected mouse model was established via rapid tail vein injection of pGL3-CP-Fluc-HBV1.2_{C2} plasmid. Outcomes included body weight, HBsAg/HBV DNA levels, and luciferase activity. Kaplan–Meier analysis assessed cumulative clearance rates, while RT-qPCR tracked model-related mRNA dynamics in PBMCs.

Results The model identified GATA3, FOXP3, IFNG, TNF, and HAVCR2 as key genes, demonstrating robust predictive accuracy for HBV clearance. Dose-specific temporal patterns of immune gene regulation were observed, revealing distinct immunomodulatory mechanisms between groups.

Conclusion This study establishes a reliable immune-based predictive model for HBV clearance and highlights divergent immune responses in chronic versus resolved infection.

Introduction

Hepatitis B virus (HBV), the causative agent of hepatitis B, is a leading cause of chronic hepatitis B (CHB), liver cirrhosis, and hepatocellular carcinoma (HCC) worldwide [1]. According to the World Health Organization, more than 296 million people are chronically infected with HBV, with 1.5 million new infections occurring annually [2]. The persistent liver damage caused by CHB leads to progressive liver inflammation, extensive fibrosis, and even cancer [3]. Currently, chronic HBV infection is the primary cause of HCC in China, imposing a significant burden on patients, families, and society [4].

The interaction between HBV replication and the host immune system determines the outcome of infection, either acute clearance of HBV or chronic HBV

†Rongzheng Zhang, Han Qiao and Kun Zhou these authors contributed equally to this work.

*Correspondence:
Shuyun Zhang
ZSY600799@hrbmu.edu.cn
[1] Scientific Research Center, The Second Affiliated Hospital of Harbin Medical University, Harbin 150000, China
[2] Department of Clinical Laboratory, Beidahuang Industry Group General Hospital, Harbin 150000, China
[3] Department of Clinical Laboratory, The First Clinical Hospital of Jilin Academy of Traditional Chinese Medicine, Changchun 130000, China
[4] Department of Immunology, Harbin Medical University, Harbin 150000, China

persistence [5]. Compared to acute HBV infection, the host immune response is significantly weaker in chronic HBV infection, making the restoration of host immune function more critical than merely suppressing viral replication [6]. Adaptive immunity plays a key role in controlling HBV infection: HBV-specific T cells are activated with the help of antigen-presenting cells (APCs) and secrete antiviral cytokines such as IFN-γ and TNF-α, which induce cytotoxic T lymphocyte (CTL) responses to kill HBV-infected hepatocytes [7]. Additionally, B cells differentiate into plasma cells under the guidance of follicular helper T (Tfh) cells, producing specific antibodies [8]. While much research has focused on the cytotoxic $CD8^+$ T cells, $CD4^+$ T cells are equally crucial for viral clearance, as the generation of effective $CD8^+$ T cells and the maintenance of functional memory T cells depend on $CD4^+$ T cells [9]. During an immune response to pathogen infection, $CD4^+$ T lymphocytes differentiate into various helper T cell subsets such as T helper 1 (Th1), T helper 2 (Th2), T helper 17 (Th17), and regulatory T cells (Treg) [10, 11]. This differentiation is driven by a set of transcription factors that either activate or repress key genes, controlling the development of different immune cell lineages. Specific transcription factors like T-box transcription factor 21 (T-bet), GATA binding protein-3 (GATA-3), RAR-related orphan receptor gamma t (RORγt), and Forkhead box P3 (Foxp3) are crucial for the development of Th1, Th2, Th17, and Treg cells, respectively [12, 13]. Cytokines, as essential components of immune function, play roles in the pathogenesis, immune exhaustion, and viral clearance in chronic HBV infection [14]. Interferons (IFNs) and tumor necrosis factors (TNFs) are particularly important in the various processes of chronic HBV infection. Recent studies have indicated that the functional exhaustion of HBV-specific T cells may be a mechanism leading to chronic HBV infection. The expression of co-inhibitory receptors on exhausted T cells increases significantly, which is closely related to T cell unresponsiveness to pathogens. Blocking these pathways can improve the function of specific T cells [15, 16].

Clinical predictive models play a crucial role in disease diagnosis and prognosis evaluation. Researchers have developed various predictive models for HBV-related liver cancer, HBV-related liver fibrosis, and HBV-related acute-on-chronic liver failure [17–19]. However, models for predicting HBV clearance have not been widely explored. Currently, there is a lack of predictive models based on immune markers for HBV clearance. Therefore, we aim to develop a predictive model for HBV clearance from the perspective of immunity, focusing on $CD4^+$ T cell subsets, cytokines, and immune checkpoint-related genes.

In addition, the host range of HBV is extremely limited, as it can only infect humans and certain primates (such as chimpanzees) but not most other species. Due to ethical constraints, the use of primate models is strictly regulated. Although ducks can be infected with duck hepatitis B virus (DHBV), the homology between DHBV and HBV is only 40%, which limits the applicability of this model in HBV research [20]. While mice cannot be naturally infected with HBV, Huang et al. successfully achieved sustained expression of HBV DNA in mouse livers using hydrodynamic injection (HI) technology [21]. Studies have shown that injecting different doses of plasmids significantly affects the duration of HBV persistence in mouse models: both insufficient and excessive doses of plasmids accelerate HBV clearance, whereas a dose of 5 μg or 6 μg results in a relatively prolonged presence of HBV in the mouse models [22, 23]. Tracking the immune dynamics of HBV-infected individuals is highly challenging; however, mouse models can simulate human HBV infection, providing a valuable platform for analyzing immune dynamics in vivo.

This study aims to explore the interrelationships between chronic HBV infection and $CD4^+$ T lymphocyte subsets, cytokines, and immune checkpoints. Additionally, we aim to develop an HBV clearance prediction model based on experimental data. Simultaneously, by establishing an HBV mouse model, we will observe the complete natural course of the disease. This approach not only aids in understanding the immunopathological mechanisms of chronic HBV infection but also allows for dynamic observation of the mutual interactions between HBV and host immunity. This research is crucial for further assessment of HBV infection status and prediction of its clearance.

Methods

Figure 1 illustrates the specific workflow of this study, aimed at enhancing readers'understanding of the research process.

Ethics approval and inclusion to participate

All research involving human participants in this study was approved by the Ethics Committee of Harbin Medical University, approval number KY27-118, in compliance with the Helsinki Declaration, and written informed consent was obtained from all participants. All experiments involving animal use were performed in accordance with the Ethics Committee of Harbin Medical University with approval number SYDW2010-144, and were conducted in accordance with the ARRIVE guidelines.

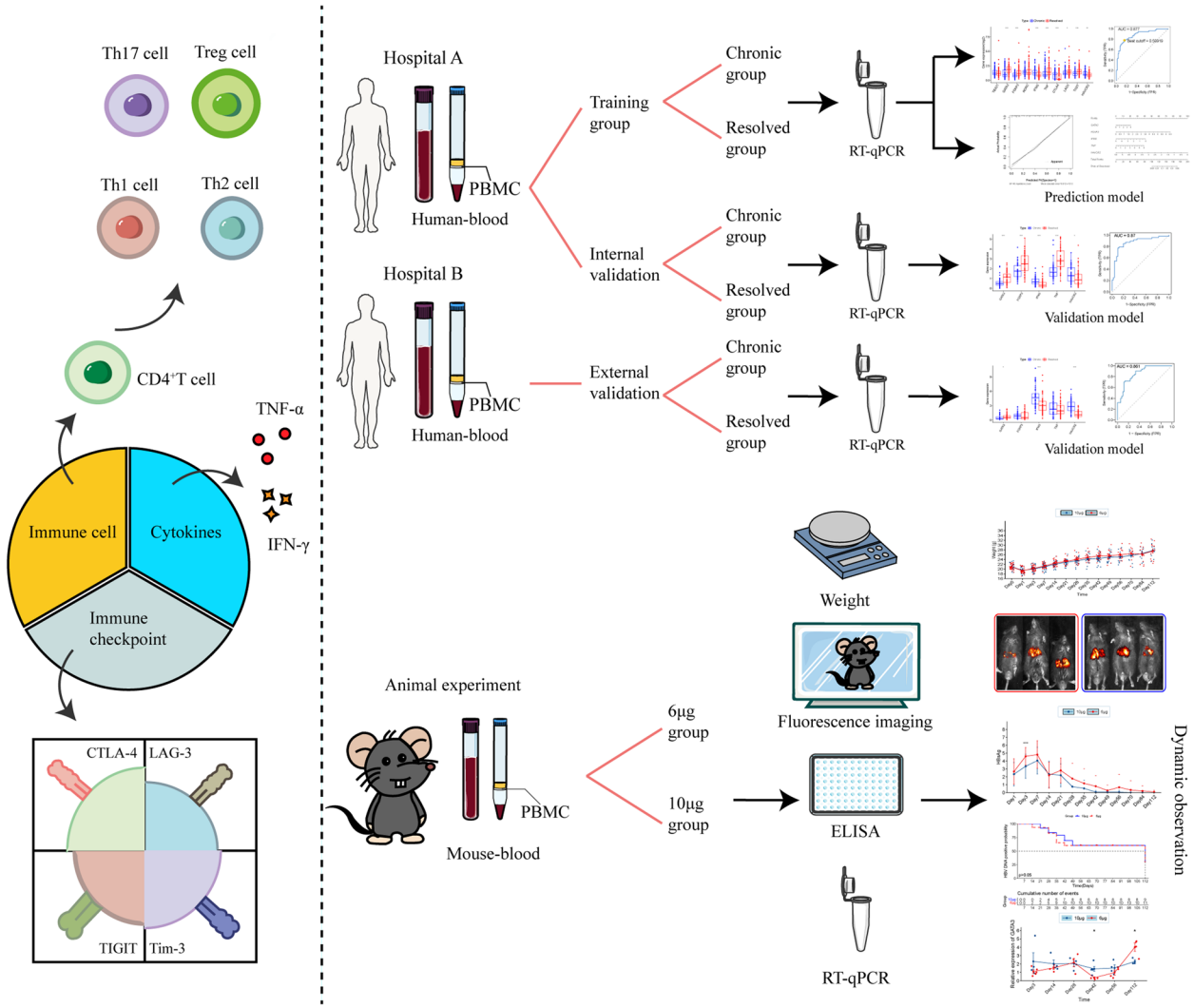

Fig. 1 Flow diagram. Hospital A: The Second Affiliated Hospital of Harbin Medical University; Hospital B: Beidahuang Industry Group General Hospital

Patients

From September 2021 to December 2022, EDTA-K_2-anticoagulated peripheral blood samples were obtained from 158 chronic HBV patients and 152 resolved HBV individuals at the Second Affiliated Hospital of Harbin Medical University. Between March 2025 and April 2025, an additional 51 chronic HBV and 50 resolved HBV individuals were similarly enrolled from Beidahuang Industry Group General Hospital. Both groups were aged over 18 years. Inclusion criteria were as follows: (1) Chronic HBV infection group: positive serum HBsAg and/or HBV DNA for more than 6 months; (2) Resolved HBV group: negative HBsAg, with positive HBsAb, HBeAb, and HBcAb, or positive HBeAb and HBcAb alone or together. Exclusion criteria included: (1) Concurrent infection with other viruses; (2) Presence of other serious physical or mental illnesses; (3) Use of interferon drugs, corticosteroids, immunosuppressants, or chemotherapy drugs. Clinical diagnosis and research procedures adhered to the Helsinki Declaration. Written informed consent was obtained from all participants involved in this study.

Plasmid

Based on the HBV C2 subtype full genome sequence (GenBank: JQ688404.1) and the pAAV/HBV1.2 plasmid constructed by Huang et al. [21], we employed gene synthesis and homologous recombination methods. Specifically, we utilized the 1.2-fold HBV gene sequence (nt1400-nt3182/1-nt1987) from the pAAV/HBV1.2

plasmid as a basis. The target sequence, comprising the complete 1.2-fold HBV gene segment with ITRs at both ends, was split and designed with adjacent overlapping primers covering the target sequence. PCR amplification yielded the complete 1.2-fold HBV gene segment with ITRs. This segment was then recombined into the destination vector pGL3-CP-Fluc (Mlu I/Xho I enzyme-cut vector) using homologous recombination, resulting in the recombinant plasmid pGL3-CP-Fluc-HBV1.2c2 containing both the reporter gene and the 1.2-fold HBV genome. The experimental procedures were conducted by Beijing Liuhe Huada Genomics Institute.

Animal experiments

Male wild-type C57BL/6 mice were purchased from the Animal Experimental Center of the Second Affiliated Hospital of Harbin Medical University or Changsheng Biotechnology. They were housed under specific pathogen-free conditions with a 12-h light/dark cycle. The pGL3-CP-Fluc-HBV1.2$_{C2}$ plasmid was transfected into the liver of mice via HI to establish an HBV mouse model [21]. D-luciferin potassium salt (ST198, Beyotime, China) was injected into the mouse peritoneal cavity, and the mice were placed in a prone position under a live animal imaging system (Burker, Switzerland) for 3 min to detect the expression intensity of luciferase. Mouse body weight was measured at different time points, and blood samples were collected.

Real-time quantitative polymerase chain reaction (RT-qPCR)

Patient PBMCs were isolated as in previous studies [24]. Mouse PBMCs were isolated using Mouse PBMC Isolation Kit (LDS1090, TBDscienceHY, China). Total RNA from PBMCs was extracted using RNAkey™ Reagent (SM129-02, Sevenbio, China). 1 μg of RNA was converted to cDNA using All-in-one First Strand cDNA Synthesis Kit II (SM143-02, Sevenbio, China). RT-qPCR was performed using SYBR Green Master Mix (SM143-01, Sevenbio, China) and an RT-qPCR instrument (SLAN-96p, Shanghai hongshi, China). ΔCT values were normalized to β-actin. HBV DNA detection was conducted using HBV Nucleic Acid Quantitative Detection Kit (SANSURE BIOTECH, China) following the manufacturer's instructions. Primer sequences are listed in Supplementary Table 1.

Enzyme-linked immunosorbent assay (ELISA)

After centrifuging at 1091 g for 15 min, mouse plasma samples were obtained. The plasma was then diluted 20-fold and HBsAg was detected using an ELISA kit (Wantai, Beijing, China), following the manufacturer's instructions. The optical density (OD) values of the sample wells were measured using an microplate reader (BIO-RAD, America) at dual wavelengths of 450 nm and 630 nm.

Bioinformatics analysis

In order to understand the chromosomal positions of the target genes, we used the R package"RCircos"for visualization. The gene chromosomal location information was obtained from the National Center for Biotechnology Information (NCBI) database. Next, to determine the potential functions and pathway mechanisms of the target genes, we conducted Gene Ontology (GO) and Kyoto Encyclopedia of Genes and Genomes (KEGG) enrichment analysis using R packages"clusterProfiler","org.Hs.eg.db","enrichplot", and"ggplot2". Enrichment results were filtered with criteria of $P < 0.05$ and adjusted P value < 0.05.

Statistical analysis

This study employed R (version 4.2.2) and GraphPad (version 9.1) for statistical analysis and graphing. Normally distributed metric data are presented as mean ± standard deviation (x ± s), while non-normally distributed metric data are presented as median and interquartile range. Student's t-test or Mann–Whitney U test was used for comparing data between two groups. For comparisons among multiple groups, One-Way ANOVA test, Kruskal–Wallis test, or Tamhane's T2 test was used, with Bonferroni correction applied for pairwise comparisons. Spearman test was used for correlation analysis. Chi-square test was used for comparing two rates or proportions. ROC curves were used to assess the diagnostic performance of genes or models. Binary logistic regression analysis was conducted for multifactorial analysis, stepwise selection was used for variable screening, variance inflation factor (VIF) was checked to detect collinearity among variables, and calibration curves and column charts were plotted. The analyses and visualizations utilized R packages including"pheatmap","limma","pROC","fmsb","SimDesign","tdROC","rmda","rms","regclass","ResourceSelection", and"ggplot2". A significance level of $P < 0.05$ was considered statistically significant.

Results

Demographic characteristics and clinical features

According to the above inclusion criteria, a total of 209 chronic HBV patients and 202 resolved HBV individuals were included in this study. Table 1 summarizes their clinical characteristics. Comparison between patient groups from the two medical institutions revealed statistically significant differences in ALT ($P < 0.001$) and AST ($P < 0.01$) levels, whereas no significant difference was observed in gender distribution ($P >$

Table 1 Clinical characteristics of study participants

Characteristics	The Second Affiliated Hospital of Harbin Medical University			Beidahuang Industry Group General Hospital		
	Chronic group ($n=158$)	Resolved group ($n=152$)	*P* value	Chronic group ($n=51$)	Resolved group ($n=50$)	*P* value
Male/Female	79/79	88/64	0.111	25/26	17/33	0.126
Age	46.50 (35.00–53.25)	50.00 (42.25–55.00)	< 0.001	55.00 (47.00–61.00)	52.00 (42.25–58.25)	0.142
ALT(u/l)	37.00 (21.00–74.00)	18.00 (14.00–27.00)	< 0.001	24.00 (18.00–37.00)	16.50 (12.00–22.25)	< 0.001
AST(u/l)	30.00 (20.00–59.25)	19.00 (15.00–24.00)	< 0.001	23.00 (18.00–35.00)	19.50 (16.00–23.00)	0.006

Table 2 Clinical Characteristics of training and internal validation group participants

Characteristics	Training group ($n=212$)	Internal validation group ($n=98$)	*P* value
Chronic/Resolved	108/104	50/48	0.990
Male/Female	115/97	52/46	0.846
Age	49.00 (39.00–54.00)	48.00 (35.75–53.25)	0.243
ALT(u/l)	24.50 (16.00–42.75)	26.00 (16.75–47.25)	0.548
AST(u/l)	21.00 (16.00–32.75)	25.00 (18.00–38.25)	0.06

Table 3 Clinical Characteristics of training group participants

Characteristics	Chronic group ($n=108$)	Resolved group ($n=104$)	*P* value
Male/Female	54/54	61/43	0.206
Age	45.50 (34.25–52.00)	51.00 (44.25–56.75)	< 0.001
ALT(u/l)	36.50 (21.25–72.50)	17.00 (14.00–26.00)	< 0.001
AST(u/l)	28.00 (20.00–56.00)	18.00 (15.00–23.75)	< 0.001

0.05). Notably, a significant age difference was found between chronic HBV patients and those in the remission group from the Second Affiliated Hospital of Harbin Medical University ($P < 0.001$).

According to the order of enrollment, participants from the Second Affiliated Hospital of Harbin Medical University were divided into a training group (the first 70%) and a internal validation group (the remaining 30%) at a 7:3 ratio. As shown in Table 2, there were no statistically significant differences in baseline characteristics, including gender distribution, age, and ALT and AST levels, between the two groups (all $P > 0.05$).

Tables 3 and 4 present the baseline characteristics of participants in the training group and the internal validation group, respectively. In the training group,

Table 4 Clinical Characteristics of internal validation group participants

Characteristics	Chronic group ($n=50$)	Resolved group ($n=48$)	*P* value
Male/Female	25/25	27/21	0.535
Age	47.50 (35.75–54.25)	49.00 (35.25–51.00)	0.909
ALT(u/l)	37.50 (21.00–75.75)	19.50 (14.00–34.75)	< 0.001
AST(u/l)	34.50 (21.75–60.75)	21.00 (16.00–26.00)	< 0.001

compared with the resolved HBV group, the chronic HBV infection group showed significant differences in age ($P < 0.001$), ALT ($P < 0.001$), and AST ($P < 0.001$) levels, while no significant difference was observed in gender distribution ($P > 0.05$). In the internal validation group, ALT ($P < 0.001$) and AST ($P < 0.001$) levels differed significantly between the chronic and resolved groups, whereas age and gender distribution showed no statistically significant differences ($P > 0.05$). In summary, the training-validation stratification effectively preserved balanced baseline parameters between the study cohorts.

Bioinformatics analysis of the target genes

To gain a clearer understanding of the ten target genes included in this study, their positions were visualized using a circos plot (Fig. 2A). Through GO analysis, enrichment analysis revealed that in the Biological Process (BP) section, they are mainly enriched in pathways such as regulation of leukocyte cell–cell adhesion. In the Cellular Component (CC) section, enrichment was observed primarily on the external side of plasma membrane. In the Molecular Function (MF) section, enrichment was noted in activities such as DNA-binding transcription repressor activity, RNA polymerase II-specific (Fig. 2B). Additionally, KEGG analysis showed that the target genes are predominantly enriched in pathways

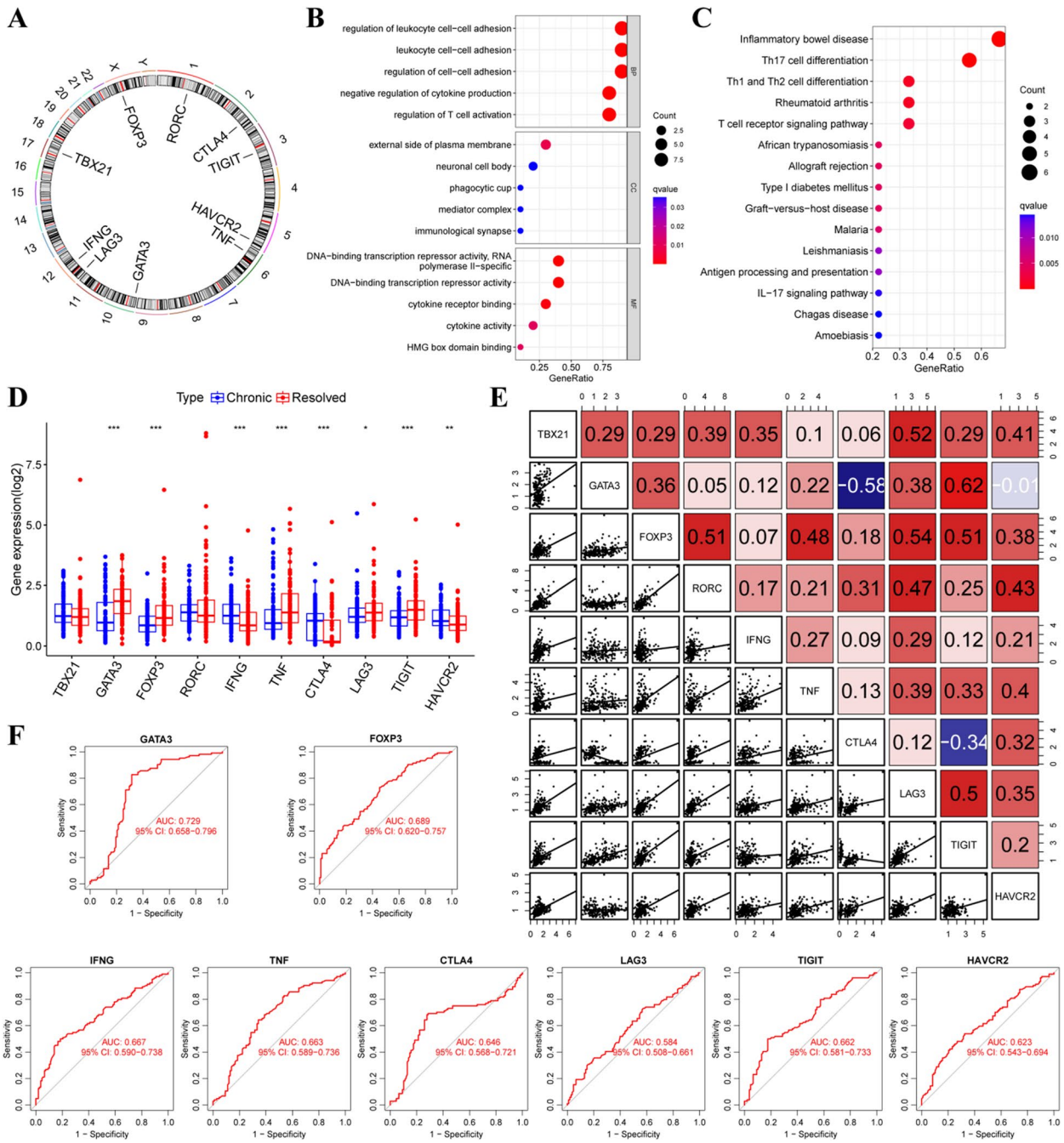

Fig. 2 Bioinformatics analysis and identification of DEGs. **A** Circular map of the chromosomal positions of ten genes. **B** The bubble plot of GO enrichment analysis. **C** The bubble plot of KEGG pathway enrichment analysis. **D** The boxplot of mRNA expression of ten genes. **E** Correlation plot of mRNA expression of eight genes. **F** ROC curve of eight genes

related to Th17, Th1, and Th2 cell differentiation, as well as T-cell receptor (TCR) signaling (Fig. 2C).

Identifying differentially expressed genes (DEGs)

Using RT-qPCR, mRNA levels of 10 genes were assessed in 212 PBMC samples from the training group, including 108 chronic HBV-infected individuals and 104 resolved HBV individuals. In the resolved group, expression levels of GATA3 ($P < 0.001$), FOXP3 ($P < 0.001$), TNF ($P < 0.001$), LAG3 ($P = 0.034$), and TIGIT ($P < 0.001$) were significantly higher compared to the chronic group, while expression levels of IFNG ($P < 0.001$), CTLA4 ($P < 0.001$),

and HAVCR2 (P = 0.002) were significantly lower than the chronic group. TBX21 and RORC did not show statistically significant differences (Fig. 2D). In correlation analysis, most gene expressions were positively correlated, with FOXP3 showing higher correlations with TNF (R = 0.48), LAG3 (R = 0.54), and TIGIT (R = 0.51). TIGIT exhibited high correlations with GATA3 (R = 0.62) and LAG3 (R = 0.5). GATA3 and CTLA4 showed a significant negative correlation (R = −0.58) (Fig. 2E). ROC analysis demonstrated that the AUC values for GATA3, FOXP3, IFNG, TNF, CTLA4, LAG3, TIGIT, and HAVCR2 were 0.729, 0.689, 0.667, 0.663, 0.646, 0.584, 0.662, and 0.5623, respectively (Fig. 2F). These results indicate that the expression levels of the target genes are correlated and possess diagnostic potential.

Development and evaluation of prediction models for HBV clearance

First, we included eight markers (GATA3, FOXP3, IFNG, TNF, CTLA4, LAG3, TIGIT, and HAVCR2) that showed statistical differences into the model and conducted logistic regression analysis. The results are shown in Fig. 3A, where CTLA4, LAG3, and TIGIT did not exhibit statistical differences. Subsequently, using AIC as the selection criterion, we employed backward elimination to select variables. The final model included five markers (GATA3, FOXP3, IFNG, TNF, and HAVCR2) (Fig. 3B). The model formula is *P = 1/[1 + e^(-(−0.34 + 0.854*GATA3 expression + 1.929*FOXP3 expression—1.367*IFNG expression + 1.075*TNF expression—2.995*HAVCR2 expression))]*.

To check for multicollinearity issues in the model, we used the VIF method, and the results are shown in Fig. 3C, where the VIF values for all five variables were significantly less than 10, indicating no significant multicollinearity among the variables. Furthermore, we evaluated the diagnostic performance of the model using ROC curve analysis. At a cutoff value of 0.50919, the model had an AUC of 0.877 (Fig. 3D). We ranked the AUCs of the prediction model and the five genes, and the model's AUC was significantly higher than that of individual markers (Fig. 3E).

Additionally, we used calibration curves to assess the model, and the results are shown in Fig. 3F, demonstrating close agreement between predicted and actual outcomes. Subsequently, based on the five variables, we constructed nomograms to personalize the assessment of HBV clearance probability for each patient. Scores for each marker were derived based on their expression values, and these scores were summed to determine the total score and thereby assess clearance probability (Fig. 3G).

Validation of the HBV clearance prediction model

We used RT-qPCR to detect mRNA levels of model genes in 98 PBMC samples from an internal validation cohort, including 50 patients with chronic HBV infection and 48 resolved HBV individuals. In the resolved group, the expression levels of GATA3, FOXP3, and TNF were significantly higher than those in the chronic group ($P < 0.001$), while the expression levels of IFNG ($P < 0.001$) and HAVCR2 ($P < 0.05$) were lower than those in the chronic group, consistent with the trends observed in the training cohort (Fig. 4A). ROC analysis showed an AUC of 0.87 for the test cohort (Fig. 4B).

To evaluate the generalizability and robustness of the model, an independent external cohort from Beidahuang Group General Hospital, comprising 51 chronic HBV patients and 50 resolved HBV individuals, was used for external validation. The results showed that, compared to the chronic group, resolved group exhibited significantly higher GATA3 mRNA expression levels ($P < 0.05$), while IFNG ($P < 0.001$) and HAVCR2 ($P < 0.05$) expression levels were significantly lower (Fig. 4C). ROC curve analysis demonstrated an AUC of 0.861 in this external validation cohort (Fig. 4D). Although the magnitude of gene expression differences was slightly attenuated compared to the internal validation cohort, the model still exhibited strong discriminatory performance.

Dynamic observation of HBV transfected mice

Building upon established dose-dependent effects of plasmid transfection on HBV persistence (6 μg: prolonged infection; 20 μg: rapid clearance), we selected intermediate plasmid doses of 6 μg (persistence-favoring) and 10 μg (moderate-clearance) for comparative analysis. The pGL3-CP-Fluc-HBV1.2$_{C2}$ plasmids were dissolved in sterile saline at these concentrations and HI into mice to establish HBV-transfected murine models. The body weight was measured, and peripheral blood was collected regularly (Fig. 5A). As shown in Fig. 5B, there were no statistically significant differences in initial body weights or at each time point among the two groups ($P > 0.05$). Following injection, mice exhibited a significant initial weight loss on 1 day post-infection (DPI) ($P < 0.001$), which gradually increased thereafter. By the 3 DPI, weights were higher than on the 1 DPI ($P < 0.01$), and by 7 DPI, weights were higher than on 3 DPI ($P < 0.001$), with no statistical difference between initial and 7 DPI weights, indicating recovery to initial weight levels by 7 DPI (Fig. 5C).

We collected peripheral blood from mice at specified time points for HBsAg and HBV DNA detection. There was no statistical difference in HBsAg levels between the two groups on 1 DPI, but on 3 DPI, HBsAg

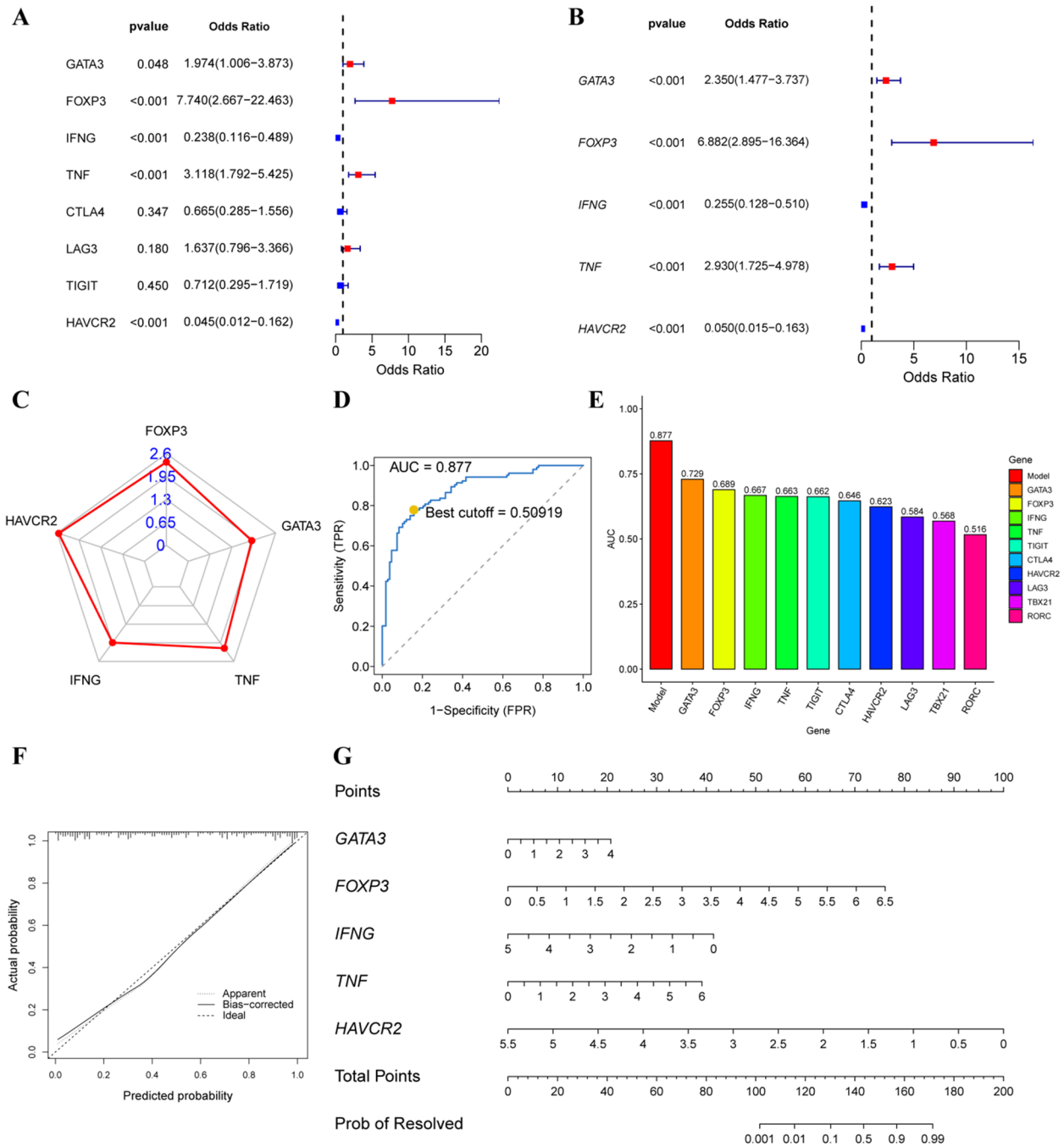

Fig. 3 Development and evaluation of prediction models for HBV clearance. **A** The forest plot of logistic regression analysis. **B** The forest plot of logistic regression analysis after variable selection using backward elimination. **C** The radar plot of variance inflation factor values. **D** The ROC curve of the prediction model. **E** The bar graph comparing the AUC of the prediction model with five genes. **F** The calibration plot of the model. **G** The nomogram showing the inclusion of five variables

levels were significantly higher in the 6 μg group compared to the 10 μg group ($P < 0.001$). Starting from 7 DPI, HBsAg levels gradually decreased in both groups over time (Fig. 5D, Figure S1 A). Kaplan–Meier curves showed cumulative rates of HBsAg clearance in mice, and there was a statistically significant difference in clearance times between the two groups ($P < 0.05$), with mice in the 6 μg group requiring longer time for HBsAg clearance (Fig. 5E).

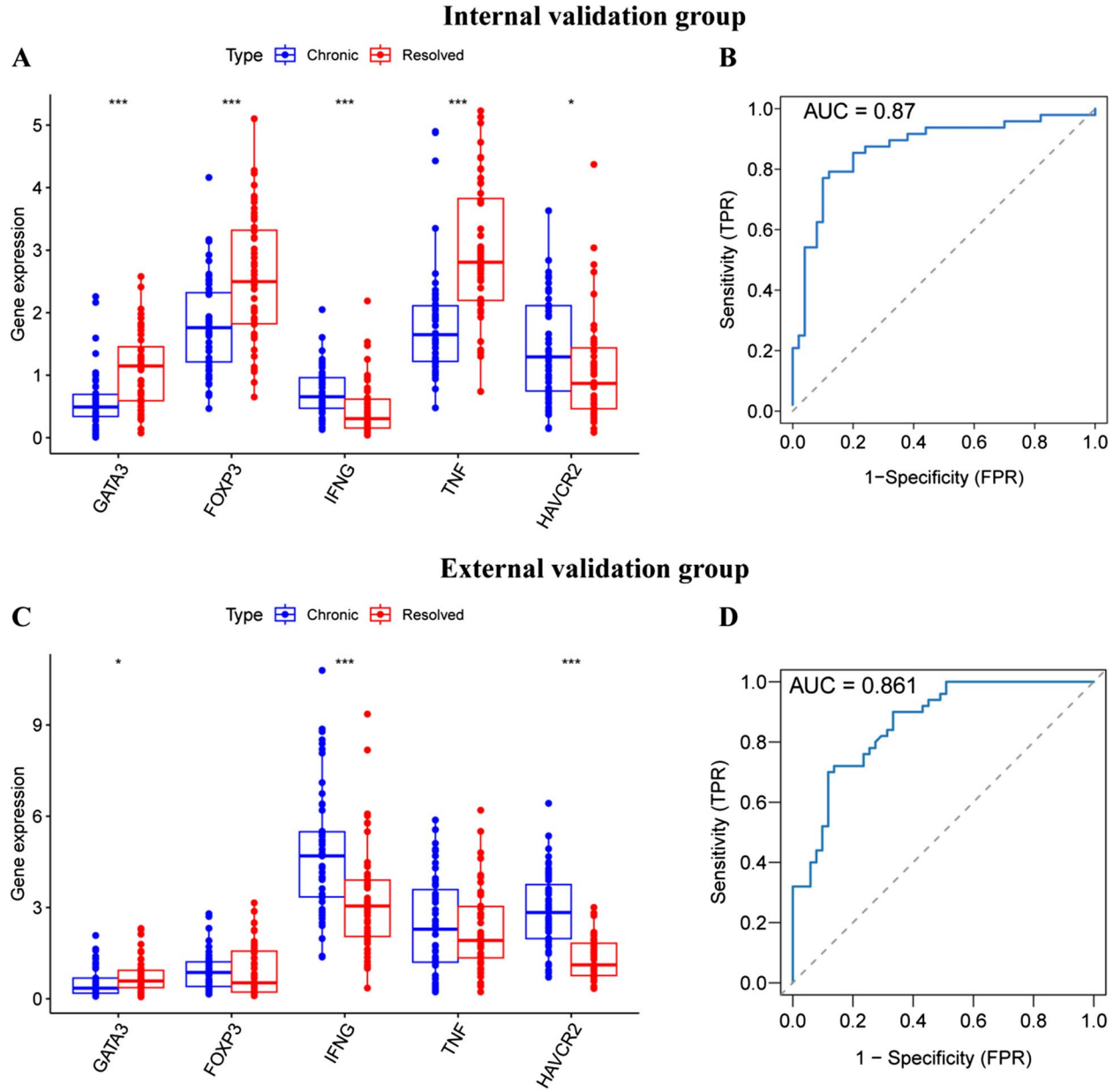

Fig. 4 Validation of the HBV clearance prediction model. **A** The boxplot of mRNA expression of model genes in the internal validation group. **B** The ROC curve of the prediction model in the internal validation group. **C** The boxplot of mRNA expression of model genes in the external validation group. **D** The ROC curve of the prediction model in the external validation group

In both matched 6 μg and 10 μg groups, there was a significant increase in HBsAg levels on 3 DPI compared to 1 DPI ($P < 0.05$). However, there was no statistical difference in HBsAg levels between 3 and 7 DPI, while HBsAg levels significantly decreased on 14 DPI compared to 7 DPI (Figures S1B-C).

Regarding HBV DNA detection, HBV DNA levels were significantly higher in the 6 μg group compared to the 10 μg group on 7 DPI and 35 DPI ($P < 0.01$). HBV DNA levels gradually decreased over time starting from 1 DPI in both groups (Fig. 5F, Figures S1D-F). Kaplan–Meier curves for HBV DNA clearance showed no statistically significant difference in clearance times between the two groups ($P > 0.05$), indicating a longer presence of HBV DNA in peripheral blood compared to HBsAg (Fig. 5G).

To observe the expression of pGL3-CP-Fluc-HBV1.2$_{C2}$ plasmids in the liver of mice, we performed dynamic observations using live fluorescence imaging.

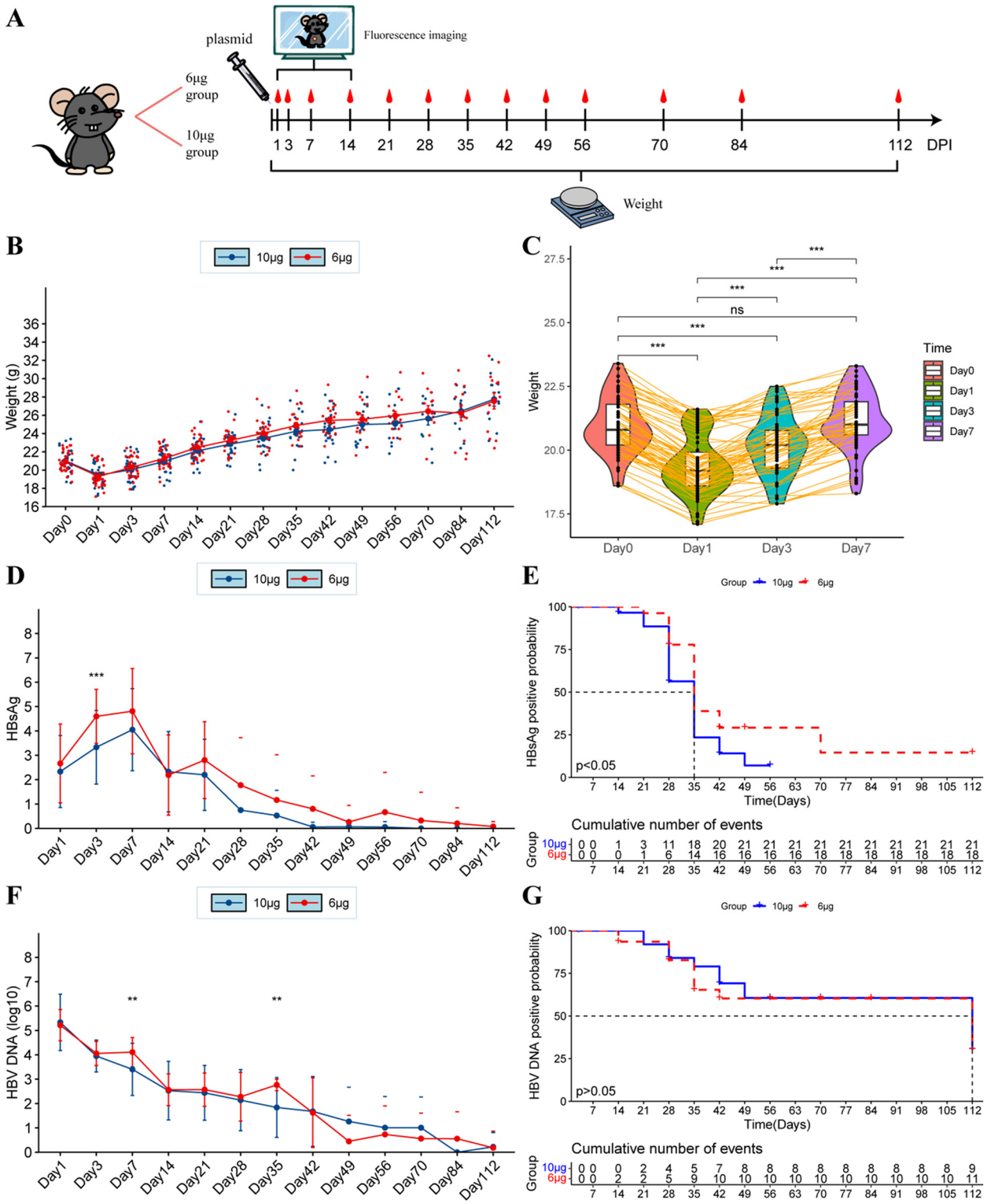

Fig. 5 Dynamic observations of body weight, HBsAg, and HBV DNA levels in HBV-transfected mice. **A** The schematic diagram of in HBV transfection mice experiment. **B** The line graph of mice body weight. **C** The violin plot of paired mouse body weights. **D** The line graph of HBsAg. **E** The Kaplan–Meier curves showed cumulative rates of HBsAg clearance in mice. **F** The line graph of HBV DNA. **G** The Kaplan–Meier curves showed cumulative rates of HBV DNA clearance in mice. The 6 μg group and 10 μg group represent mice injected with 6 μg and 10 μg of the pGL3-CP-Fluc-HBV1.2$_{C2}$ plasmid, respectively

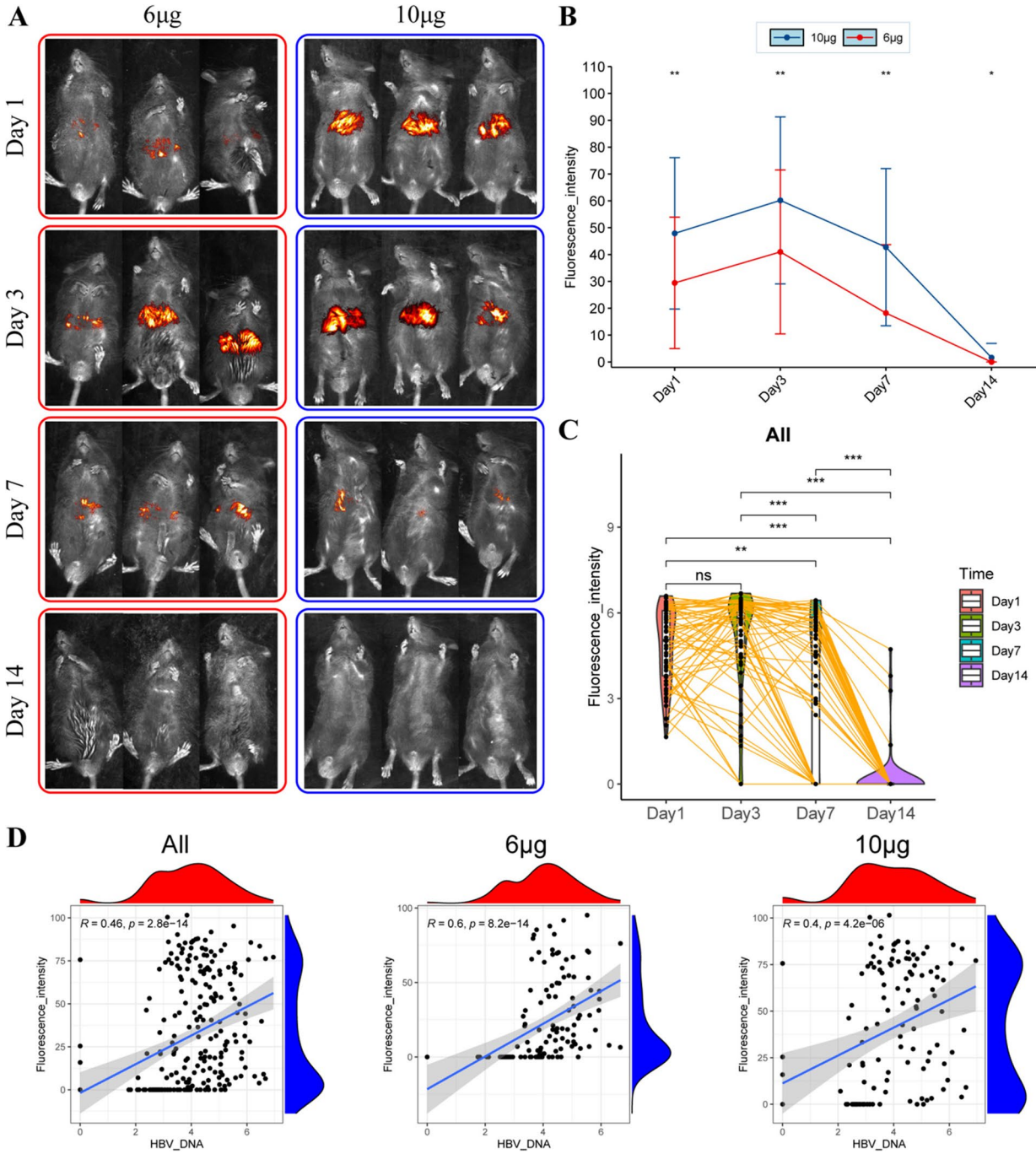

Fig. 6 Dynamic observation of fluorescence intensity in HBV-transfected mice. **A** Fluorescence intensity at different time points in two groups of mice. **B** The line graph of fluorescence intensity. **C** The violin plot of paired mouse fluorescence intensity. **D** Correlation analysis between fluorescence intensity and HBV DNA

Fluorescence intensity in the 10 μg group was significantly higher than in the 6 μg group on 1 DPI($P < 0.01$), 3 DPI ($P < 0.01$), 7 DPI ($P < 0.01$), and 14 DPI ($P < 0.05$) (Fig. 6A, B). In all mice, there was a trend of increased fluorescence intensity on 3 DPI compared to 1 DPI, but it was not statistically significant ($P > 0.05$), while fluorescence intensity significantly decreased on 7 DPI ($P < 0.001$), and most mice showed disappearance of fluorescence by 14 DPI (Fig. 6C, Figures S1G-H). In correlation analysis, HBV DNA levels correlated positively with

fluorescence intensity (r = 0.46, $P < 0.001$), with higher correlation observed in the 6 μg group (r = 0.6, $P < 0.001$) compared to the 10 μg group (r = 0.4, $P < 0.001$) (Fig. 6D).

In summary, our findings confirm that 6 μg plasmid dosing generates a durable HBV persistence model, creating conditions for longitudinal immune gene expression profiling.

The mRNA expression levels of model genes in PBMCs of HBV-transfected mice

At the designated time points, euthanasia was performed on the mice, and blood samples were collected. PBMCs were isolated, and the mRNA levels of target genes were detected using RT-qPCR. To elucidate the dynamic changes of HBV DNA, HBsAg, and immune-related genes, we performed longitudinal analyses in both the 6 μg and 10 μg groups. In the 6 μg group, we observed a gradual increase in TNF expression accompanying the progressive decline of HBV DNA and HBsAg levels. Notably, IFNG and HAVCR2 exhibited transient fluctuations at 28 DPI, while GATA3 showed a biphasic pattern at 42 DPI, with an initial increase followed by a significant decrease and then a rebound ($P < 0.05$). FOXP3 expression was markedly upregulated at both 56 DPI and 112 DPI (Fig. 7A). In contrast, although HBV DNA and HBsAg also declined gradually in the 10 μg group, most immune genes remained relatively stable without a sustained upward trend. However, transient peaks in IFNG and HAVCR2 were detected at 12 DPI, and TNF fluctuated repeatedly throughout the observation period (Fig. 7B). Comparative analysis revealed significant differences in the temporal expression patterns between the two groups. The 6 μg group exhibited more dynamic immune modulation, with GATA3 significantly downregulated at 42 DPI ($P < 0.05$) and upregulated at 112 DPI ($P < 0.05$), and FOXP3 elevated at 14 DPI ($P < 0.05$). Notably, TNF expression rebounded at 28 and 56 DPI ($P < 0.05$) in this group. In contrast, no significant intergroup differences in HAVCR2 expression were observed at any time point (Fig. 7C). These findings demonstrate a temporal pattern of immune gene regulation, suggesting that the 6μg and 10μg groups may involve distinct immunomodulatory mechanisms during HBV clearance.

Discussion

CHB, as a global public health issue, is associated with approximately one-third of cirrhosis cases and half of hepatocellular carcinoma cases [25]. The natural course of chronic HBV infection is primarily determined by changes in virus-host immune interactions, characterized by varying viral loads, e-antigen status, and degree of liver damage at different clinical stages [26]. The mechanisms underlying persistent viral infection depend not only on the biological characteristics of the virus itself but also on the host's immune response status.

In this study, we established an immune-based predictive model for HBV clearance, identifying GATA3/FOXP3/IFNG/TNF/HAVCR2 as key determinants through multicenter validation. Notably, our murine studies revealed dose-specific temporal patterns of these markers, suggesting distinct immunoregulatory mechanisms between chronic and resolved infections.

The immunological mechanisms underlying HBV clearance appear to involve complex interactions among multiple immune cell populations. GATA-3 plays a pivotal role in Th2 cell differentiation, with its expression potentially regulated through the IL-4/STAT6 pathway while being reciprocally inhibited by Th1 cell activity. This balanced Th1/Th2 response in individuals with resolved infection likely facilitates B cell activation and restoration of humoral immune function, as supported by previous studies [27, 28]. The Foxp3 expression patterns observed in our study present an intriguing paradox. While chronic HBV infection typically demonstrates increased Treg cell frequency, our resolved cases exhibited a distinct temporal pattern of Foxp3 regulation. We hypothesize that this may represent a compensatory mechanism whereby transient Treg expansion helps mitigate immune-mediated liver damage without compromising the development of HBV-specific CD8 + T cells or memory T cells [29, 30]. Elevated IFNG expression in the HBV-infected group may reflect that some patients were in the immune clearance phase or active disease stage. This interpretation is supported by clinical characteristics showing significantly higher ALT and AST levels in the chronic group compared to the self-limited group, suggesting ongoing hepatic inflammation. The dual role of inflammatory cytokines in HBV infection was particularly evident in our results. TNF-α and IFN-γ demonstrated divergent associations—while elevated TNF-α levels in PBMCs showed strong correlation with viral clearance, increased IFN-γ levels were more significantly associated with hepatic inflammation. This dichotomy underscores the delicate balance between viral control and immunopathology in HBV infection [31]. Our data further reveal unexpected patterns in immune checkpoint expression. Contrary to conventional exhaustion markers observed in chronic infections, the resolved group exhibited downregulation of CTLA-4 and TIM-3 alongside elevated LAG3 and TIGIT expression. This surprising finding challenges current paradigms and suggests these molecules may play more nuanced roles in HBV clearance than previously recognized [32]. The distinct expression profiles of these immune regulators in resolved versus chronic infections point to potentially

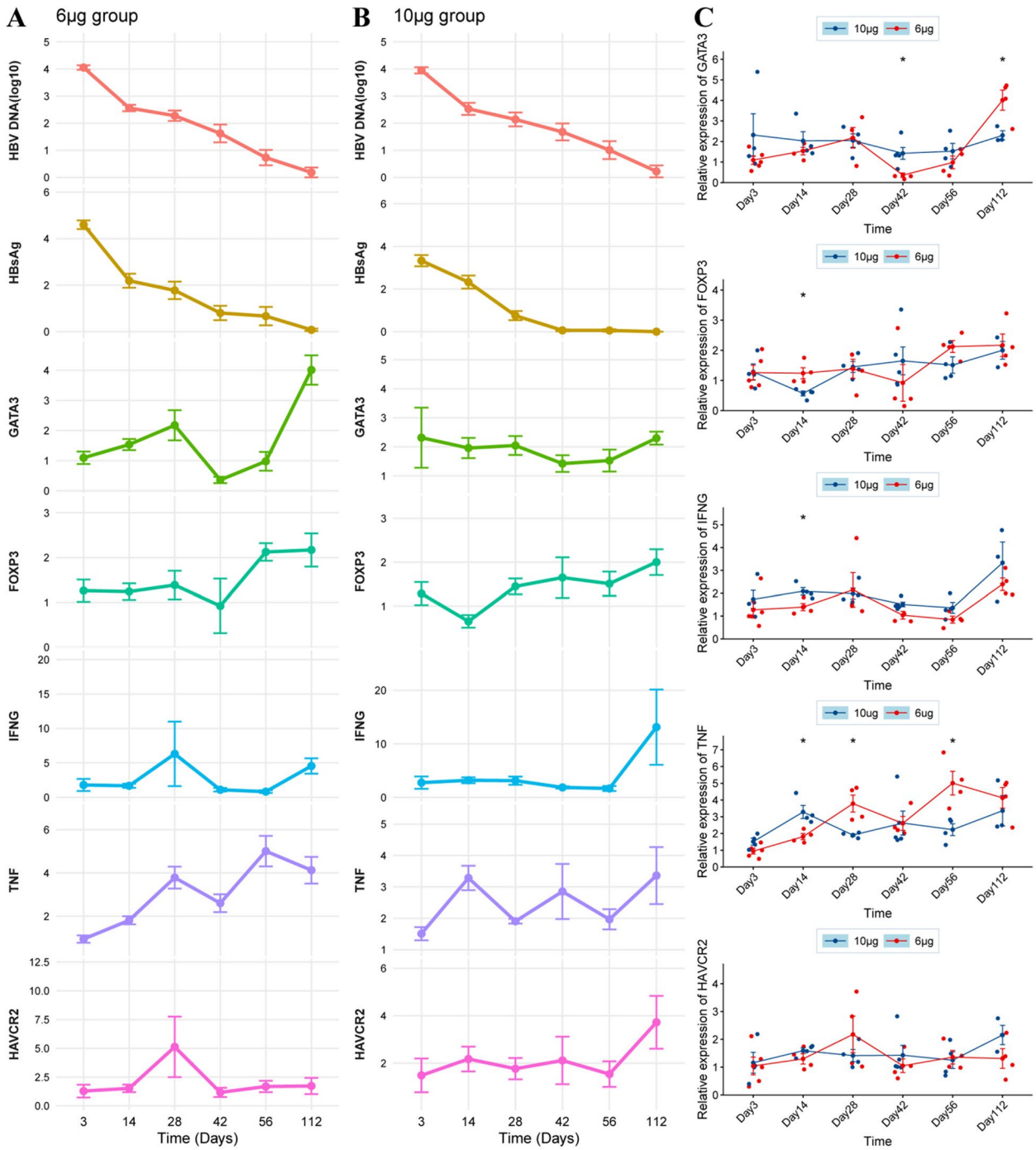

Fig. 7 Dynamic observation of model gene expression levels in HBV-transfected mice. **A** The line graph illustrating the dynamic changes in HBV DNA, HBsAg, and model gene expression levels in the 6 μg group. **B** The line graph illustrating the dynamic changes in HBV DNA, HBsAg, and model gene expression levels in the 10 μg group. **C** The line graph of model gene mRNA expression levels at different time points in two groups of mice

novel mechanisms of viral control that warrant further investigation.

The development of reliable mouse models for HBV and host immune system research represents a critical advancement in the field. In our study, we successfully established a robust experimental system by hydrodynamically injecting varying concentrations (6 μg and 10 μg) of the pGL3-CP-Fluc-HBV1.2$_{C2}$ plasmid into mouse livers, enabling comprehensive dynamic monitoring of viral and immunological parameters. The transient body

weight reduction observed immediately post-injection, followed by complete recovery without mortality, confirms the procedure's safety and aligns with previous reports of minimal adverse effects [33]. Our virological analyses revealed several important findings regarding HBV dynamics. Both experimental groups exhibited peak HBsAg levels approximately one week post-injection, consistent with the kinetics reported for pAAV/HBV 1.2 plasmid transfection [22]. While the 6 μg group demonstrated higher HBsAg levels at 3 DPI—a finding that initially appears counterintuitive regarding dose response—this observation actually corroborates Wang et al.'s report of similar initial HBsAg levels following 6 μg and 20 μg injections [23]. The apparent discrepancy between fluorescence intensity (consistently higher in the 10 μg group) and HBsAg levels may reflect fundamental differences in viral protein translation efficiency, secretion kinetics, or stability, though the precise mechanisms require further investigation. The immunological implications of our findings are particularly noteworthy. The Kaplan–Meier analysis clearly demonstrated faster HBsAg clearance in the 10 μg group, supporting previous observations that higher plasmid doses correlate with accelerated viral clearance [23]. This phenomenon mirrors clinical observations in chimpanzee models, where high-dose HBV exposure results in limited hepatocyte infection and reduced immune-mediated liver damage compared to low-dose exposure [34]. Our model's recapitulation of the well-documented clinical pattern of HBV DNA clearance lagging behind HBsAg clearance further validates its physiological relevance [35]. The live imaging data provided unique insights into early viral replication events, with fluorescence intensity peaking at 3 DPI—notably preceding the HBsAg peak. This temporal pattern reflects the molecular cascade of HBV replication: initial plasmid-driven transcription of pgRNA and other viral mRNAs, formation of replication intermediates, subsequent protein translation, and eventual secretion—processes that necessarily introduce measurable delays between plasmid delivery and detectable antigenemia. This comprehensive murine model successfully captures multiple key aspects of human HBV infection and clearance dynamics while offering unique advantages for real-time monitoring of viral activity. The dose-dependent effects observed in our system provide valuable insights for understanding immune-viral interactions and may inform future therapeutic strategies aimed at modulating these responses.

Our longitudinal analysis revealed that distinct plasmid doses can shape qualitatively different immune landscapes, ultimately influencing the kinetics and outcomes of HBsAg clearance. Mice receiving 6 μg plasmid developed a more prolonged but regulated immune response, characterized by sustained expression of GATA3, FOXP3, and TNF. This profile may reflect a more tolerogenic or modulated immune environment, potentially delaying viral clearance despite activation of key immune pathways. In contrast, the 10 μg group mounted an earlier and more pro-inflammatory response—marked by elevated IFNG and TNF and reduced FOXP3 expression at the critical 14-day post-immunization point—which likely accelerated antigen clearance. TNF, in particular, may play a central role in mediating these differences. It exerts antiviral activity through multiple mechanisms, including reducing viral entry into hepatocytes, disrupting nucleocapsids leading to cccDNA decay, and indirectly suppressing HBV transcription and replication by modulating cellular FLICE-inhibitory protein (c-FLIP) [36–38]. The earlier upregulation of TNF in the 10 μg group may therefore contribute mechanistically to its more efficient viral clearance, whereas delayed TNF induction in the 6 μg group could explain its slower resolution.

These findings point to a dose-dependent immune polarization, where lower doses may favor balanced immune activation and regulatory feedback, while higher doses drive stronger inflammatory responses that more effectively eliminate the virus. Importantly, the biphasic pattern of GATA3 in the 6 μg group hints at dynamic Th2 involvement over time, further underscoring the complex interplay between immune regulation and antiviral efficacy. Taken together, our data suggest that even with identical antigenic content, the magnitude of immune stimulation profoundly alters host-virus interactions, tipping the balance between persistence and clearance. This highlights the importance of immunogen dosage not only for response magnitude but also for qualitative immune trajectory—a key consideration for optimizing therapeutic vaccine design against HBV.

Although this study provides valuable insights, several limitations should be acknowledged. First, when collecting information from the two groups of participants, it was not possible to precisely determine their time of HBV infection or the exact timing of HBV clearance. Second, the single-center design and regional restriction of our study population may limit the generalizability of our findings. Regarding the animal experiments, although we conducted a comprehensive longitudinal analysis, the limited volume of peripheral blood in individual animals posed technical constraints that prevented us from tracking PBMC profiles from the same mouse across different time points. As a result, different mice had to be used at each time point, which may have introduced inter-individual variability. Nevertheless, our study has significant strengths that mitigate these limitations. The predictive model was developed using a large sample size and was rigorously validated in an independent cohort. Importantly, the conserved expression

patterns of GATA3 and TNF between the 6 μg mouse group and human PBMCs strongly suggest their crucial role in the mechanism of HBsAg clearance. This cross-species consistency enhances the biological relevance of our findings and supports their potential translational value.

Conclusions

We selected 5 genes—GATA3, FOXP3, IFNG, TNF, and HAVCR2—as model genes and developed a model for predicting HBV infection clearance based on their mRNA expression, demonstrating good predictive capability. We observed the natural course of HBV infection using an HBV-transfected mouse model.

Supplementary Information

The online version contains supplementary material available at https://doi.org/10.1186/s12985-025-02792-w.

Supplementary Material 1.

Acknowledgements
Not applicable.

Authors' contributions
Z.R. conceived the experiment. Z.R., J.X., C.X. and Q.H. conducted the experiment. W.M. helped with manuscript editing. Y.L. contributed to data curation. Z.R. and D.J. performed statistical analysis and figure generation. Z.R., and Z.K. wrote the initial draft of the manuscript. Z.S. reviewed and edited the manuscript. Z.S. supervised the project. All authors reviewed the manuscript.

Funding
The present study was supported by Special Fund for Clinical Research of Wu Jieping Medical Foundation (320.6750.18230).

Data availability
No datasets were generated or analysed during the current study.

Declarations

Ethics approval and consent to participate
All research involving human participants in this study was approved by the Ethics Committee of Harbin Medical University, approval number KY27-118, in compliance with the Helsinki Declaration, and written informed consent was obtained from all participants. All experiments involving animal use were performed in accordance with the Ethics Committee of Harbin Medical University with approval number SYDW2010-144, and were conducted in accordance with the ARRIVE guidelines.

Consent for publication
Not applicable.

Competing interests
The authors declare no competing interests.

Received: 24 January 2025 Accepted: 13 May 2025
Published online: 21 May 2025

References

1. Robinson A, Wong R, Gish RG. Chronic Hepatitis B Virus and Hepatitis D Virus: New Developments. Clin Liver Dis. 2023;27(1):17–25. https://doi.org/10.1016/j.cld.2022.08.001.
2. WHO. Hepatitis B Key facts. 2022. Available: https://www.who.int/news-room/fact-sheets/detail/hepatitis-b.
3. Yu R, Fan R, Hou J. Chronic hepatitis B virus infection: epidemiology, prevention, and treatment in China. Front Med. 2014;8(2):135–44. https://doi.org/10.1007/s11684-014-0331-5.
4. Chan HL, Sung JJ. Hepatocellular carcinoma and hepatitis B virus. Semin Liver Dis. 2006;26(2):153–61. https://doi.org/10.1055/s-2006-939753.
5. Rouse BT, Sehrawat S. Immunity and immunopathology to viruses: what decides the outcome? Nat Rev Immunol. 2010;10(7):514–26. https://doi.org/10.1038/nri2802.
6. Zheng JR, Wang ZL, Feng B. Hepatitis B functional cure and immune response. Front Immunol. 2022;13:1075916. https://doi.org/10.3389/fimmu.2022.1075916.
7. You CR, Lee SW, Jang JW, Yoon SK. Update on hepatitis B virus infection. World J Gastroenterol. 2014;20(37):13293–305. https://doi.org/10.3748/wjg.v20.i37.13293.
8. Wang X, Dong Q, Li Q, et al. Dysregulated Response of Follicular Helper T Cells to Hepatitis B Surface Antigen Promotes HBV Persistence in Mice and Associates With Outcomes of Patients. Gastroenterology. 2018;154(8):2222–36. https://doi.org/10.1053/j.gastro.2018.03.021.
9. Buschow SI, Jansen DTSL. CD4 T Cells in Chronic Hepatitis B and T Cell-Directed Immunotherapy. Cells. 2021;10(5):1114. https://doi.org/10.3390/cells10051114+.
10. Kallies A, Good-Jacobson KL. Transcription Factor T-bet Orchestrates Lineage Development and Function in the Immune System. Trends Immunol. 2017;38(4):287–97. https://doi.org/10.1016/j.it.2017.02.003.
11. Yu D, Rao S, Tsai LM, et al. The transcriptional repressor Bcl-6 directs T follicular helper cell lineage commitment. Immunity. 2009;31(3):457–68. https://doi.org/10.1016/j.immuni.2009.07.002.
12. Lazarevic V, Glimcher LH, Lord GM. T-bet: a bridge between innate and adaptive immunity. Nat Rev Immunol. 2013;13(11):777–89. https://doi.org/10.1038/nri3536.
13. Tanriver Y, Diefenbach A. Transcription factors controlling development and function of innate lymphoid cells. Int Immunol. 2014;26(3):119–28. https://doi.org/10.1093/intimm/dxt063.
14. Zhong S, Zhang T, Tang L, Li Y. Cytokines and Chemokines in HBV Infection. Front Mol Biosci. 2021;8: 805625. https://doi.org/10.3389/fmolb.2021.805625.
15. Nakamoto N, Cho H, Shaked A, et al. Synergistic reversal of intrahepatic HCV-specific CD8 T cell exhaustion by combined PD-1/CTLA-4 blockade. PLoS Pathog. 2009;5(2): e1000313. https://doi.org/10.1371/journal.ppat.1000313.
16. Raziorrouh B, Schraut W, Gerlach T, et al. The immunoregulatory role of CD244 in chronic hepatitis B infection and its inhibitory potential on virus-specific CD8+ T-cell function. Hepatology. 2010;52(6):1934–47. https://doi.org/10.1002/hep.23936.
17. Hu Z, Yuan Y, Hu Z, et al. Development and Validation of Prognostic Nomograms for Hepatocellular Carcinoma After Hepatectomy Based on Inflammatory Markers. J Hepatocell Carcinoma. 2022;9:1403–13. https://doi.org/10.2147/JHC.S390858.
18. Xie G, Wang X, Wei R, et al. Serum metabolite profiles are associated with the presence of advanced liver fibrosis in Chinese patients with chronic hepatitis B viral infection. BMC Med. 2020;18(1):144. https://doi.org/10.1186/s12916-020-01595-w.
19. Hou Y, Zhang Q, Gao F, et al. Artificial neural network-based models used for predicting 28- and 90-day mortality of patients with hepatitis B-associated acute-on-chronic liver failure. BMC Gastroenterol. 2020;20(1):75. https://doi.org/10.1186/s12876-020-01191-5.
20. Dandri M, Petersen J. Animal models of HBV infection. Best Pract Res Clin Gastroenterol. 2017;31(3):273–9. https://doi.org/10.1016/j.bpg.2017.04.014.
21. Huang LR, Wu HL, Chen PJ, Chen DS. An immunocompetent mouse model for the tolerance of human chronic hepatitis B virus infection. Proc Natl Acad Sci U S A. 2006;103(47):17862–7. https://doi.org/10.1073/pnas.0608578103.

22. Li L, Li S, Zhou Y, et al. The dose of HBV genome contained plasmid has a great impact on HBV persistence in hydrodynamic injection mouse model. Virol J. 2017;14(1):205. https://doi.org/10.1186/s12985-017-0874-6.
23. Wang X, Zhu J, Zhang Y, et al. The doses of plasmid backbone plays a major role in determining the HBV clearance in hydrodynamic injection mouse model. Virol J. 2018;15(1):89. https://doi.org/10.1186/s12985-018-1002-y.
24. Zhang R, Xia Y, Dong J, et al. Comprehensive Analysis of m7G-Related Genes and Chronic Hepatitis B: Diagnostic Markers, Immune Microenvironment Regulation. Disease Progression J Immunol Res. 2023;2023:9471520. https://doi.org/10.1155/2023/9471520.
25. Perz JF, Armstrong GL, Farrington LA, Hutin YJ, Bell BP. The contributions of hepatitis B virus and hepatitis C virus infections to cirrhosis and primary liver cancer worldwide. J Hepatol. 2006;45(4):529–38. https://doi.org/10.1016/j.jhep.2006.05.013.
26. Croagh CM, Lubel JS. Natural history of chronic hepatitis B: phases in a complex relationship. World J Gastroenterol. 2014;20(30):10395–404. https://doi.org/10.3748/wjg.v20.i30.10395.
27. Zheng W, Flavell RA. The transcription factor GATA-3 is necessary and sufficient for Th2 cytokine gene expression in CD4 T cells. Cell. 1997;89(4):587–96. https://doi.org/10.1016/s0092-8674(00)80240-8.
28. Zhu J, Min B, Hu-Li J, et al. Conditional deletion of Gata3 shows its essential function in T(H)1-T(H)2 responses. Nat Immunol. 2004;5(11):1157–65. https://doi.org/10.1038/ni1128.
29. Zhang M, Zhou J, Zhao T, et al. Dissection of a circulating and intrahepatic CD4(+)Foxp3(+) T-cell subpopulation in chronic hepatitis B virus (HBV) infection: a highly informative strategy for distinguishing chronic HBV infection states. J Infect Dis. 2012;205(7):1111–20. https://doi.org/10.1093/infdis/jis011.
30. Stross L, Günther J, Gasteiger G, et al. Foxp3+ regulatory T cells protect the liver from immune damage and compromise virus control during acute experimental hepatitis B virus infection in mice. Hepatology. 2012;56(3):873–83. https://doi.org/10.1002/hep.25765.
31. Xia Y, Stadler D, Lucifora J, et al. Interferon-γ and Tumor Necrosis Factor-α Produced by T Cells Reduce the HBV Persistence Form, cccDNA. Without Cytolysis Gastroenterology. 2016;150(1):194–205. https://doi.org/10.1053/j.gastro.2015.09.026.
32. Attanasio J, Wherry EJ. Costimulatory and Coinhibitory Receptor Pathways in Infectious Disease. Immunity. 2016;44(5):1052–68. https://doi.org/10.1016/j.immuni.2016.04.022.
33. Huang M, Sun R, Huang Q, Tian Z. Technical Improvement and Application of Hydrodynamic Gene Delivery in Study of Liver Diseases. Front Pharmacol. 2017;8:591. https://doi.org/10.3389/fphar.2017.00591.
34. Asabe S, Wieland SF, Chattopadhyay PK, et al. The size of the viral inoculum contributes to the outcome of hepatitis B virus infection. J Virol. 2009;83(19):9652–62. https://doi.org/10.1128/JVI.00867-09.
35. Wu W, Liu Y, Lin Y, et al. PreC and C Regions of Woodchuck Hepatitis Virus Facilitate Persistent Expression of Surface Antigen of Chimeric WHV-HBV Virus in the Hydrodynamic Injection BALB/c Mouse Model. Viruses. 2017;9(2):35. https://doi.org/10.3390/v9020035.
36. Watashi K, Liang G, Iwamoto M, Marusawa H, Uchida N, Daito T, Kitamura K, Muramatsu M, Ohashi H, Kiyohara T, Suzuki R, Li J, Tong S, Tanaka Y, Murata K, Aizaki H, Wakita T. Interleukin-1 and tumor necrosis factor-α trigger restriction of hepatitis B virus infection via a cytidine deaminase activation-induced cytidine deaminase (AID). J Biol Chem. 2013;288(44):31715–27. https://doi.org/10.1074/jbc.M113.501122.
37. Puro R, Schneider RJ. Tumor necrosis factor activates a conserved innate antiviral response to hepatitis B virus that destabilizes nucleocapsids and reduces nuclear viral DNA. J Virol. 2007;81(14):7351–62. https://doi.org/10.1128/JVI.00554-07.
38. Park YK, Park ES, Kim DH, Ahn SH, Park SH, Lee AR, Park S, Kang HS, Lee JH, Kim JM, Lee SK, Lim KH, Isorce N, Tong S, Zoulim F, Kim KH. Cleaved c-FLIP mediates the antiviral effect of TNF-α against hepatitis B virus by dysregulating hepatocyte nuclear factors. J Hepatol. 2016;64(2):268–77. https://doi.org/10.1016/j.jhep.2015.09.012.

Publisher's Note